ΕΘΝΙΚΟ ΜΕΤΣΟΒΙΟ ΠΟΛΥΤΕΧΝΕΙΟ
ΔΙΑΤΜΗΜΑΤΙΚΟ ΠΡΟΓΡΑΜΜΑ ΜΕΤΑΠΤΥΧΙΑΚΩΝ ΣΠΟΥΔΩΝ
«ΣΥΣΤΗΜΑΤΑ ΑΥΤΟΜΑΤΙΣΜΟΥ»

Μεταπτυχιακή Εργασία

CONTROL OF THE MOBILE PLATFORM OF A MOBILE ROBOTIC GAIT REHABILITATION SYSTEM

ΚΥΡΑΡΙΝΗ ΜΑΡΙΑ

Επιβλέπων Καθηγητής: Κωνσταντίνος Κυριακόπουλος

ΑΘΗΝΑ 2014

ABSTRACT

In this thesis, an inverse kinematics based control algorithm for joystick control of the mobile platform of the CORBYS mobile robot-assisted gait rehabilitation system is presented. An inverse kinematics based algorithm generates the steering angle and the driving angular velocity for each of the four wheels of the platform, using the linear and angular velocities of the mobile platform. The thesis work is focused on the development of a control algorithm using fuzzy logic controller for steering control and PI controller for driving control of the mobile platform. The experimental results of the real-world steering and driving of the platform are also presented in the thesis.

ΠΕΡΙΛΗΨΗ

Στη παρούσα μεταπτυχιακή εργασία παρουσιάζεται ένας αλγόριθμος ελέγχου, βασισμένος στην αντίστροφη κινηματική ανάλυση, για τον έλεγχο της κινητής πλατφόρμας του CORBYS κινητού συστήματος υποβοηθούμενης αποκατάστασης βάδισης με χειριστήριο. Τα αποτελέσματα του αλγόριθμου ελέγχου, που είναι βασισμένος στην αντίστροφη κινηματική ανάλυση, είναι η γωνία διεύθυνσης και η ταχύτητα περιστροφής για κάθε ένα από τους τέσσερις τροχούς της κινητής πλατφόρμας, χρησιμοποιώντας ως είσοδο του αλγορίθμου την γραμμική και γωνιακή ταχύτητα της κινητής πλατφόρμας. Η παρούσα μεταπτυχιακή εργασία επικεντρώνεται στην ανάπτυξη ενός αλγορίθμου ελέγχου, χρησιμοποιώντας ελεγκτή ασαφούς λογικής για τον έλεγχο της γωνίας διεύθυνσης και PI-ελεγκτή για τον έλεγχο της ταχύτητας οδήγησης της κινητής πλατφόρμας. Τα πειραματικά αποτελέσματα από την κινητή πλατφόρμα για τη οδήγηση και περιστροφή της πλατφόρμας παρουσιάζονται επίσης στην παρούσα εργασία.

ACKNOWLEDGEMENTS

I would like to express my deepest appreciation to all those who provided me the possibility to complete this thesis. I would like to thank Prof. Dr. Axel Gräser and Dr. Konstantinos Kyriakopoulos for providing me the opportunity to complete my thesis in Institute of Automation, University of Bremen, as Erasmus student.

I would like to express my gratitude to my supervisors, Dr. Danijela Ristić-Durrant and Sinisa Slavnić, whose guidance, assistance and support helped me in completing my thesis.

Last but not the least, I would like to thank my friends, family and colleagues for their support and encouragement.

Table of Contents

1 Introduction

1.1 Motivation

The objective of the integrated EU FP7 project CORBYS [1] [2] is to design and implement a generic robot control architecture that allows the integration of high-level cognitive modules to support the functioning of the robot in dynamic environments including interaction with humans. As a practical application of the control architecture, a novel cognitive mobile gait rehabilitation system is being developed during the project's lifetime. Fig. 1 shows the final CAD model image of the CORBYS robot-assisted mobile gait rehabilitation system with an associated global coordinate system. It consists of an omnidirectional mobile platform, a powered robotic orthosis attached to the platform via a pelvis link, and a linear unit. The mobile platform provides mobility for a patient and enables overground walking training, whilst the powered robotic orthosis helps the patient to complete his/her leg movements.

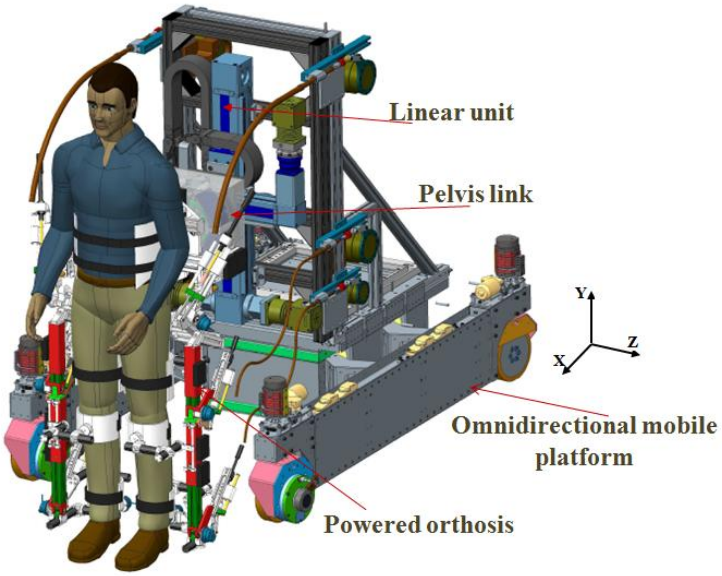

Figure 1.1 CORBYS mobile gait rehabilitation system CAD model image

The mobile platform constitutes the central housing structure of the CORBYS mobile gait rehabilitation system. It serves as a component carrier for the linear unit and motors for the orthosis, as well as the central power supply system. The mobile platform also houses a network module, and other system modules such as the safety module and the various computers upon which the modules of the control architecture run.

Four wheel hub motors are connected to the platform for driving, which provide movement of the system in x-direction. Each wheel is fitted with a steering angle motor to change its direction (rotation about y-axis) so that the platform can drive along curves.

The linear unit enables both lifting and lowering of the patient's body (patient's pelvis movement in y - direction) and side to side movement of the patient's body (patient's pelvis movement in z - direction). It is equipped with two servo-positioning motors for the actuation of the y - axis which are chosen in order to provide partial body weight support. One servo motor is used for the actuation of the z - axis.

The pelvis link is the connection between the linear unit, attached to the platform, and the powered orthosis. The pelvis link ensures that the patient's pelvis can rotate in the frontal and transverse planes. The force/torque sensor for measurement of the interaction force between the patient and the CORBYS system is placed within the pelvis link. This measurement will be used for control of the mobile platform enabling it to follow a walking patient's while he/she is wearing the powered orthosis.

The powered orthosis assists the patient's lower limb joint motions. The DoFs configuration of the CORBYS orthosis prototype follows the natural human limb kinematics. There are 6 DoFs at each leg: 3 DoFs in the hip, 1 DoF in the knee, and 2 DoFs in the ankle joints. The hip, knee and ankle joint motions on the sagittal plane (i.e. flexion and extension) are selected as active DoFs based on the biomechanical properties of human walking, while the hip DoFs in the transverse and frontal planes as well as ankle DoF in the transverse plane are passive. The movements of the orthosis joints in the sagittal plane are controlled by a

push-pull control (PPC) cable-based actuation system [3]. There are three actuators per orthosis leg that actuate the hip, knee and ankle joints in the sagittal plane. The actuators are placed on the mobile platform while the PPC cables are flexible links to the joints used to transfer the rotational movement of the motors to specifically designed orthotic joints.

1.2 Specific goal

In the fully integrated and functional CORBYS gait rehabilitation system, the mobile platform will be controlled so to follow the patient walking while wearing the orthosis. However, in the early stage of system development a joystick control of the mobile platform had to be integrated. The joystick control should enable "manual" platform control during the system development. Also, joystick control is necessary to move the platform with attached orthosis towards the patient in the process of setting up the patient in the orthosis. In this thesis, an inverse kinematics based control algorithm for joystick control of the mobile platform is presented. The inverse kinematics algorithm gives as output the steering angle and the driving angular velocity of each of the four wheels of the platform, given the linear and angular velocities of the mobile platform. The thesis is focused on the steering control of the platform for which a fuzzy logic controller was developed and implemented and on the velocity control of the platform for which a PI-controller was also developed and implemented.

The rest of the thesis is organized as follows. In section 2, the theoretical background is presented. In Section 3 the inverse kinematics model of the mobile platform used for the design of fuzzy controller and PI-controller is given. The dynamic model of the DC driving motors for the PI-controller is given in section 4. The design of fuzzy logic controller and the design of the PI-controller are given in Section 5. Section 6 presents experimental results obtained in real-world steering and driving of CORBYS mobile platform wheels using designed controllers. In the last section, the conclusion and future work are summarized.

1.3 Overview of the mobile platform system

1.3.1 Hardware overview

The automation systems comprise of sensors, actuators, computers and other I/O devices. The mobile platform of CORBYS is also an automation system. The EtherCAT protocol is used for the communication between different modules of the system. EtherCAT (Ethernet for Control Automation Technology) is an Ethernet-based fieldbus system, which was developed for low cost devices such as I/O terminals, sensors, and embedded controllers. It only uses standard Ethernet frames according to IEEE 802.3. These frames are sent by the master device and the slave devices extract and/or insert "data on the fly" [4]. The principle "data on the fly" means that data is passed by each slave device with a minimal delay before it is processed.

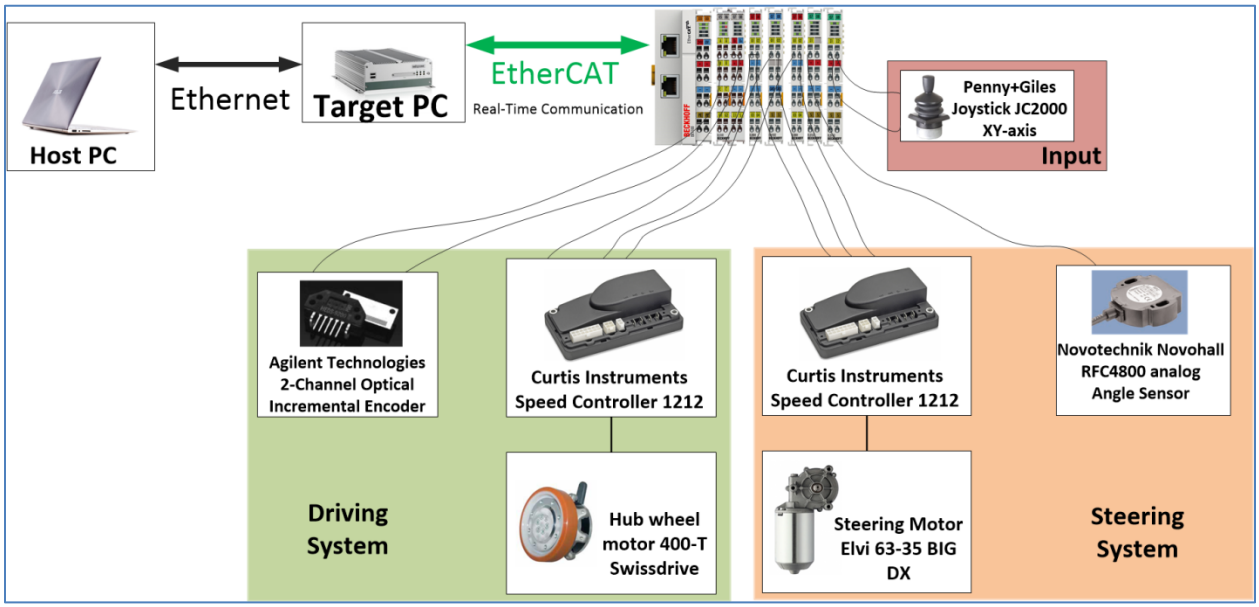

Figure 1.2 Schematic of the hardware of the mobile platform of the CORBYS mobile gait rehabilitation system.

The mobile platform of the CORBYS mobile gait rehabilitation system consists of the hardware modules (Figure 1.2):

→ *Joystick JC2000 XY-axes*

The JC2000 is a contactless joystick manufactured by Penny+Giles designed for precision fingertip control applications. It has two axes configuration, for each axis there is one analog output. The JC2000 incorporates Hall-effect sensors to detect the position of each of the joystick axes. The noise filtration has to be done later [5].

→ *Curtis 1212 motor speed controller*

The Curtis 1212 motor speed controllers provide control of permanent magnet drive motors for battery powered vehicles and they are fully programmable [6].

→ *Hub wheel motor 400-T swissdrive*

The hub wheel motor 400-T swissdrive manufactured by micromotor is a DC motor with permanent magnet [7]. The parameters of the motor are presented in chapter 3.3. Four of these motors are used for the driving system of the mobile platform. A hub wheel motor is attached to each of the wheels.

→ *Steering motor ELVI 63-35 BIG DX*

The steering motor ELVI 63-35 BIG DX manufactured by ELVI is a DC gear motor. The parameters of the motor are unknown. Four of these motors are used for the steering system of the mobile platform. A steering motor is attached to each of the wheels.

→ *Agilent Technologies HEDS-9100 Extended Resolution Series*

The HEDS-9100 from the company Agilent Technologies is a 2-channel high resolution optical incremental encoder. The encoder has two channel quadrature output. The digital output of the first channel is in quadrature with the output of the second channel (90 degrees out of phase) [8], as shown in Figure 1.3.

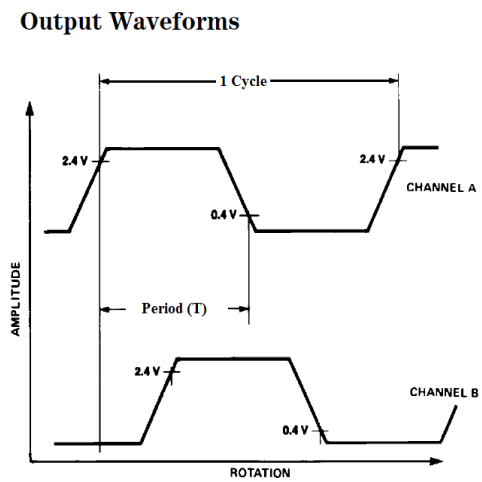

Figure 1.3 The output of the 2-channel encoder [8]

→ *Novotechnik novohall RFC4800 analog angle sensor*

The angle sensor RFC 4800 manufactured by Novotechnik utilizes a separate magnet or magnetic position marker, which has to be attached to the rotating shaft for measurement. It measures the orientation of the magnetic field, and provides the output in the form of analog signal [9]

→ *Beckhoff EtherCAT Devices*

The following EtherCAT Devices from the company Beckhoff are used in the system:

- the etherCAT Coupler EK1100 relays the communication from the higher-lever EtherCAT network to the EtherCAT terminals (ELxxxx) [10]

- the EL5101 EtherCAT Terminal is an interface for the direct connection of incremental encoders with differential input [11]

- the EL2004 4-channel digital output terminal connects the binary control signals from the automation unit on to the actuators at the process level with electrical isolation [12]

- the EL4102 2-channel analog output terminal generates signals in the range between 0 V and +10 V [13]

- the EL3161/31620 1-/2-channel analog input terminals measure input voltages from 0 to 10 V with 16-bit resolution [14].

1.3.2 Real-time software overview

The real-time application are executed by Simulink Real-Time (Formerly xPC Target) from Simulink models on a dedicated target computer hardware connected to the system hardware. It supports real-time simulation and testing, including rapid control prototyping, DSP and vision system prototyping, and hardware-in-the-loop (HIL) simulation [15].

In this thesis, algorithms for the control of the mobile platform were implemented in Simulink. In the Figure 1.2, the connection between the host-PC and the target-PC is shown. The host-PC is used for designing and modelling in Simulink. The target-PC connected with the hardware of the mobile platform, runs the Simulink model in real-time with the Simulink Real-Time.

1.4 Related work

Mobile platforms are widely used in industrial and technical applications. One of the main requirements of a mobile platform is precise mobility and manoeuvrability. In order to achieve the precision, a very accurate low level control is needed.

In this thesis, an omnidirectional indoor wheeled mobile platform is used for a gait rehabilitation system part of CORBYS (Cognitive Control Framework for Robotic Systems) project, funded by the European Commission under the 7th Framework Program in the area of Cognitive Systems and Robotics. The wheels have more degrees of freedom due to the individually actuated configuration, so separate controllers were required for each of the wheel. Different approaches have been suggested and used for control of omnidirectional wheeled mobile platforms and electric vehicles and some of them are presented below.

The study done by S. Omatu [16]for the control of speed of an electric vehicle with four independent wheels presents a neuro-PID controller (self-tuning PID controller) based on

the error back-propagation (BP) controller algorithm. The simulation results of the neuro-PID controller for speed control were almost perfect in the final stages but were not good in the initial stage, due to the learning ability of the neural networks. Additionally, in this study, for training the neural networks for various speeds, they obtained the data using a physical simulator.

Another study by Tin Lun Lam [17]shows the use of force feedback controller for the control of a four wheel independent steering vehicle. The experimental results of this study showed an error in the steering angle of the wheels.

In the work done by Xiao Ping [18] simulated annealing PID algorithm was presented, which was designed based on the transfer functions of the 4-wheel steering system, along with a comparison between the PID and the simulated annealing PID algorithm. The simulation results showed that the simulated annealing PID algorithm is providing better results in comparison to the PID.

A different study done by Norhazimi Hamzah [19] showed that the sliding mode control is able to control the steering and the driving of the Four-Wheel Active Steering Vehicle. The simulation results showed that the sliding mode control was following the reference signal exactly.

Another approach is to control an electric vehicle using fuzzy logic for steering and driving, as suggested in the study by Wang Shufeng [20]. Here the control methods: front wheel steering (FWS), zero mass-centre side-slip angle and proportional control method (4WS) and the fuzzy control method (4WS+fuzzy) were adopted. The simulation results showed that 4WS+fuzzy gives good results.

2 Theoretical Background

2.1 Fuzzy logic

Fuzzy logic was proposed by the mathematician Lofti A. Zadeh of University of California at Berkeley in 1965 [21]. Fuzzy Logic is a multivalued logic that allows intermediate values to be defined between conventional evaluations like true/false, yes/no, high/low, etc. Notions like rather tall or very fast can be formulated mathematically and processed by computers, in order to deploy a more human-like approach of thinking in the programming of computers [22].

Fuzzy logic is the logic of fuzzy sets. Lofti A. Zadeh defined the fuzzy sets as: "A fuzzy set is a class of objects with a continuum of grades of membership. Such a set is characterized by a membership (characteristic) function which assigns to each object a grade of membership ranging between zero and one" [21].

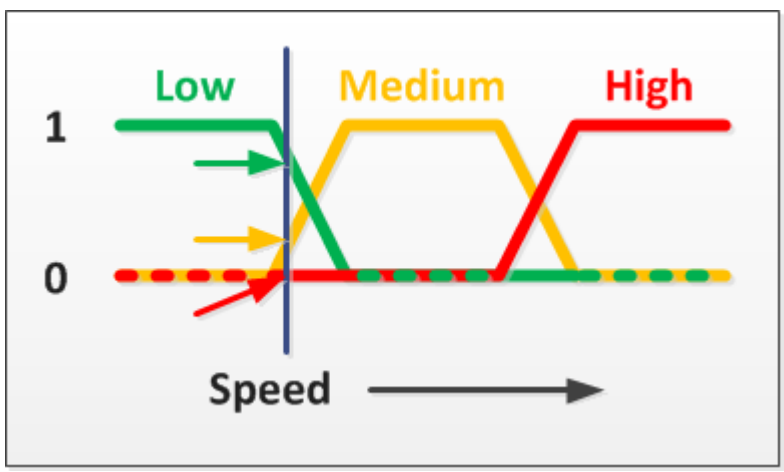

Figure 2.1 Speed membership function

Consider the example of a system that monitors the speed of a motor and indicates if the speed is low, medium or high. The system has to decide on the status of the speed (low/medium/high). For that purpose, the system has several speed membership functions - one for every speed category. As the speed is changing, its membership to some of the

functions will be weaker and to some other will be stronger, but the speed will remain a member of all the functions. The degree membership to different function is used for identification. For the particular speed shown in Figure 2.1, the description would be as "fairly low", "slightly medium" and "not high".

2.2 PID control

The PID controller is the most common form of feedback controller. The PID controller has been developed continuously for 60 years so far and it is still widely used [23].

The PID controller is a sum of thee terms: the proportional term (P-term), the integral term (I-term) and the derivative term (D-term). The proportional term is proportional to the magnitude of the error, the integral term is used to remove the steady state error of control system and improve the steady state response, the derivative term is used to predict a trend of error and improve the transient response of the system [23].By adjusting the proportional, the integral and the differential gain, the PID controller attempts to minimize the error in output. The PID control system diagram is shown in Figure 2.2.

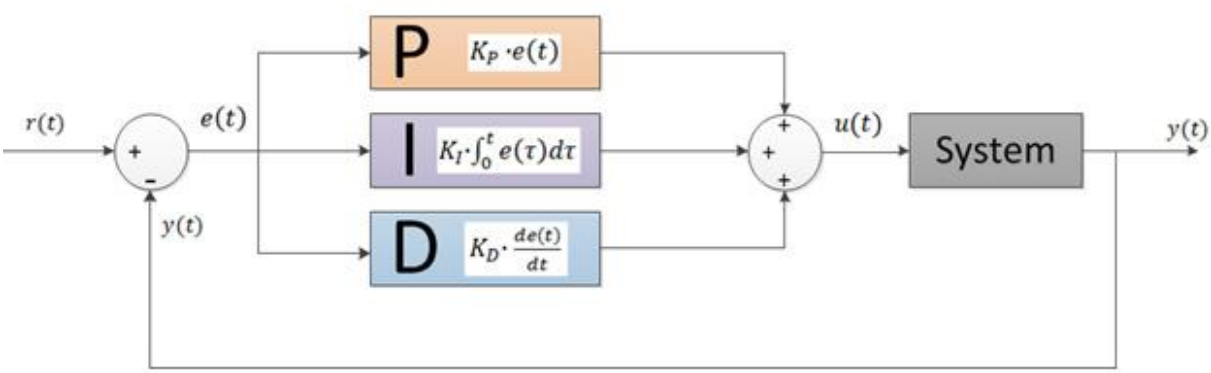

Figure 2.2 PID control system diagram

The relation between the output $u(t)$ and the input $e(t)$ of the PID controller is shown in the following equation:

$$u(t) = K_P \cdot e(t) + K_I \cdot \int_0^t e(\tau)d\tau + K_D \cdot \frac{de(t)}{dt} \tag{2.1}$$

where K_P: proportional gain, K_I: integral gain, K_D: differential gain, $u(t)$: output of PID controller, $e(t)$: error (difference) between the reference $r(t)$ and the output of the system $y(t)$.

The transfer function of the PID controller is expressed as follows:

$$G(s) = \frac{U(s)}{E(s)} = K_P + \frac{K_I}{s} + K_D \cdot s \tag{2.2}$$

3 Inverse Kinematics of the 4-wheel mobile robot

Inverse kinematics is used in robot control. Given the path for the center of mass of the mobile robot, the inverse kinematic equations calculate the steering angle of each wheel and the driving angular velocity for each wheel.

The kinematic model explained here is represented in Figure 3.1. The model of the mobile robot is a rigid body that bears four independent wheels. The wheels are represented as following:

- → *Wheel 1: Front right wheel*
- → *Wheel 2: Rear right wheel*
- → *Wheel 3: Front left wheel*
- → *Wheel 4: Rear left wheel*

The known factors for the inverse kinematic equations are the x- and z-components of linear velocity of center of mass $[V_{cx}\ ,V_{cz}]$ with respect to the inertial frame and the angular velocity of center of mass $[\omega]$ with respect to the inertial frame. The Unknown factors are the Driving angular Velocity of each wheel $[\dot{\varphi}_i$, for $= 1,2,3,4$] and the Steering Angle of each wheel $[\vartheta_i$, for $i = 1,2,3,4$]. The inverse kinematic equations can be summarized in the following expression:

$$\begin{bmatrix} \dot{\varphi}_1 \\ \dot{\varphi}_2 \\ \dot{\varphi}_3 \\ \dot{\varphi}_4 \\ \vartheta_1 \\ \vartheta_2 \\ \vartheta_3 \\ \vartheta_4 \end{bmatrix} = f^{-1}(V_{cx}, V_{cz},\ \omega) \tag{3.1}$$

For the description of the motion of the platform, the reference frames defined in the Figure 3.1 are as follows: *{O,X,Y,Z}* is inertial frame of reference, *{C,x,y,z}* is fixed to the centre of

mass of the mobile robot and $\{W_i, x_i', y_i', z_i'\}$ are fixed to the centre of each wheel. The frame $\{C, x, y, z\}$ has the unit vectors $(\mathbf{i}, \mathbf{j}, \mathbf{k})$. The wheel centre points are represented as W_i, for $i = 1,2,3,4$, as shown in Figure 3.1.

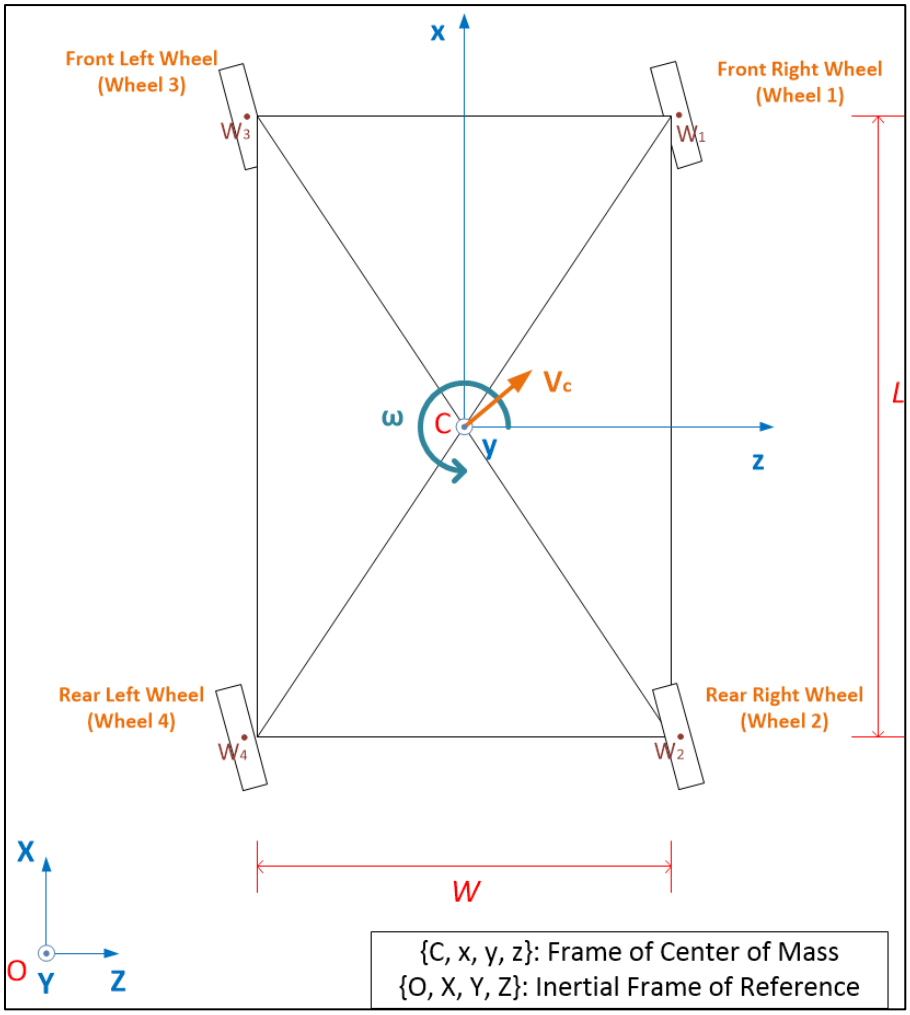

Figure 3.1 Top view of the mobile platform

The mobile platform has the following characteristics:

→ *width = 1026.4mm*

→ *length = 1702mm*

→ *wheel radius = 100mm*

The velocities $\mathbf{V}_i$ (Figure 3.2) of the wheel centre points W_i, for $i = 1,2,3,4$, with respect to the inertial frame *{O,X,Y,Z}* are calculated by the following equation:

$$\boldsymbol{V}_i = \boldsymbol{V}_c + \boldsymbol{\omega} \times \boldsymbol{d}_i + \left(\frac{\mathbf{d}(\mathbf{d}_i)}{\mathbf{dt}}\right) \tag{3.2}$$

for $i = 1,2,3,4$

where:

→ $\boldsymbol{V}_c$ *is the translation velocity of the mobile robot centre of mass, with respect to the inertial frame {O,X,Y,Z} and it has x-component and the z-component expressed in terms of the units vectors in the frame {C,x,y,z}:*

$$\boldsymbol{V}_c = \boldsymbol{V}_{cx} + \boldsymbol{V}_{cz} \tag{3.3}$$

→

→ $\boldsymbol{\omega}$ *is the angular velocity of the frame {C,x,y,z}, with respect to the inertial frame {O,X,Y,Z}. The angular velocity is positive counterclockwise* ($\boldsymbol{\omega} = \omega \boldsymbol{j}$)

→ $\boldsymbol{d}_i$ *is the position vector of the point* W_i*, with respect to the frame {C,x,y,z}*

→ $\left(\frac{\boldsymbol{d}(\boldsymbol{d}_i)}{\boldsymbol{dt}}\right)$ *is the time derivative of the position vector* $\boldsymbol{d}_i$ *and because the position vector* $\boldsymbol{d}_i$ *is constant, the time derivative equals zero*

$$\left(\frac{\mathbf{d}(\mathbf{d}_i)}{\mathbf{dt}}\right) = 0 \tag{3.4}$$

→

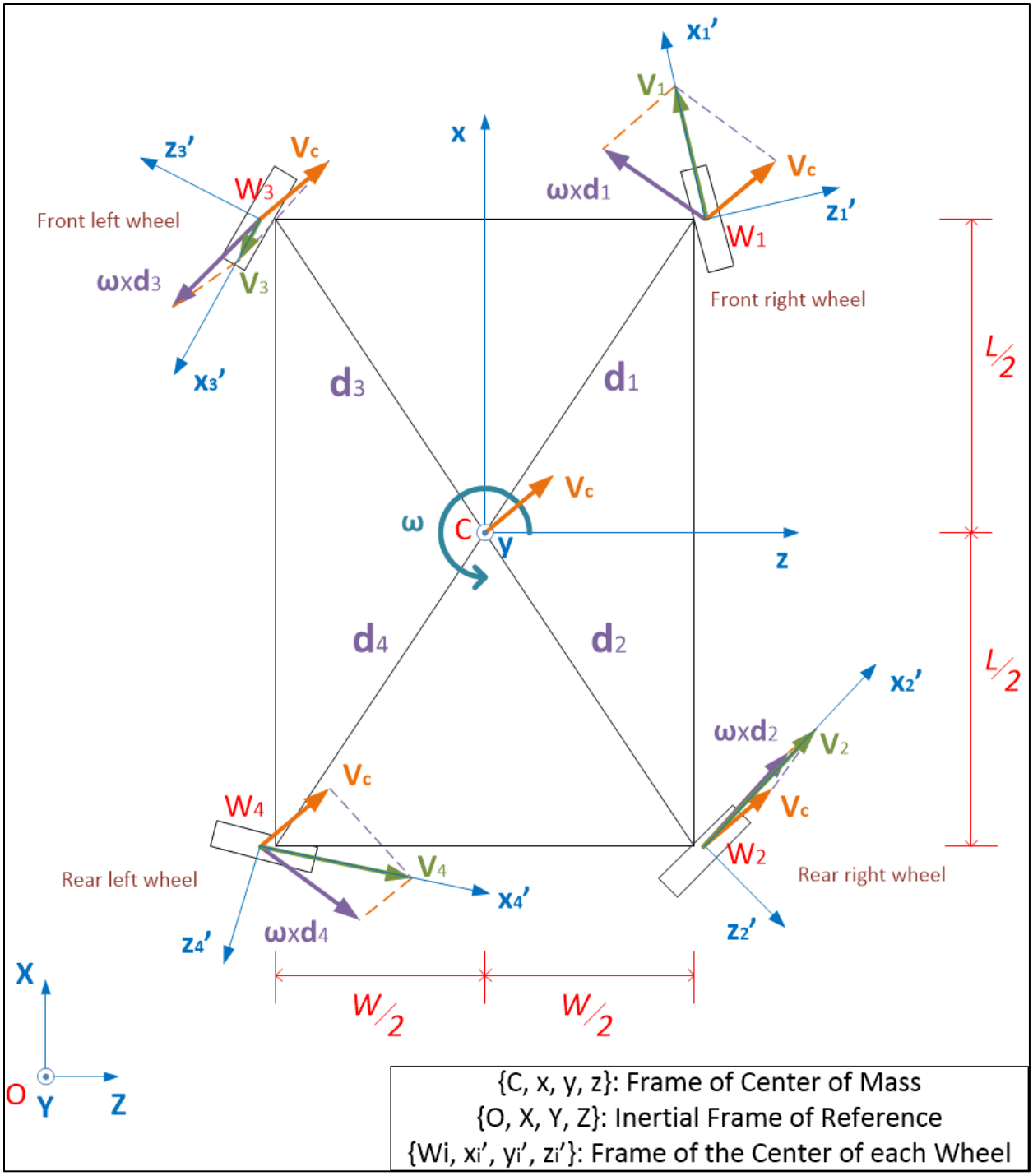

Figure 3.2 Notation of kinematics of the mobile platform (Top view)

The position vector $\boldsymbol{d}_i$, for $i = 1,2,3,4$, between the centre of the mobile robot frame and each wheel centre point can be represented as sum of the unit vectors $(\mathbf{i}, \mathbf{j}, \mathbf{k})$, with respect to the frame *{C,x,y,z}.*

$$\mathbf{d}_1 = \frac{L}{2}\mathbf{i} + \frac{W}{2}\mathbf{k} \tag{3.5}$$

$$\mathbf{d}_2 = -\frac{L}{2}\mathbf{i} + \frac{W}{2}\mathbf{k} \tag{3.6}$$

$$\mathbf{d}_3 = \frac{L}{2}\mathbf{i} - \frac{W}{2}\mathbf{k} \tag{3.7}$$

$$\mathbf{d}_4 = -\frac{L}{2}\mathbf{i} - \frac{W}{2}\mathbf{k} \tag{3.8}$$

where *W*: distance between the centres of the right and left wheels (mobile platform width), *L*: distance between the centres of the front and rear wheels (mobile platform length).

The x-component and the z-component of the velocity $\mathbf{V}_i$ (Figure 3.2) of the wheel centre points W_i, for $i = 1,2,3,4$, with respect to the inertial frame *{O,X,Y,Z}*, expressed in terms of the units vectors in the frame *{C,x,y,z},* are calculated as following:

→ *Wheel 1 - Front Right Wheel*

$$(3.2),(3.4) \xRightarrow{for\ i=1} \mathbf{V}_1 = \mathbf{V}_c + \boldsymbol{\omega} \times \mathbf{d}_1 \tag{3.9}$$

$$\xRightarrow{(3.3)(3.5)} \begin{cases} \mathbf{V}_{1x} = \mathbf{V}_{cx} + \boldsymbol{\omega} \times \left(\frac{W}{2}\mathbf{k}\right) \\ \mathbf{V}_{1z} = \mathbf{V}_{cz} + \boldsymbol{\omega} \times \left(\frac{L}{2}\mathbf{i}\right) \end{cases} \tag{3.10}$$

→ *Wheel 2 - Rear Right Wheel*

$$(3.2),(3.4) \xRightarrow{for\ i=2} \mathbf{V}_2 = \mathbf{V}_c + \boldsymbol{\omega} \times \mathbf{d}_2 \tag{3.11}$$

$$\xRightarrow{(3.3)(3.6)} \begin{cases} \mathbf{V}_{2x} = \mathbf{V}_{cx} + \boldsymbol{\omega} \times \left(\frac{W}{2}\mathbf{k}\right) \\ \mathbf{V}_{2z} = \mathbf{V}_{cz} + \boldsymbol{\omega} \times \left(-\frac{L}{2}\mathbf{i}\right) \end{cases} \tag{3.12}$$

→

→ *Wheel 3 - Front Left Wheel*

$$(3.2),(3.4) \xRightarrow{for\ i=3} \mathbf{V}_3 = \mathbf{V}_c + \boldsymbol{\omega} \times \mathbf{d}_3 \tag{3.13}$$

$$\xRightarrow{(3.3)(3.7)} \begin{cases} \mathbf{V}_{3x} = \mathbf{V}_{cx} + \boldsymbol{\omega} \times \left(-\frac{W}{2}\mathbf{k}\right) \\ \mathbf{V}_{3z} = \mathbf{V}_{cz} + \boldsymbol{\omega} \times \left(\frac{L}{2}\mathbf{i}\right) \end{cases} \tag{3.14}$$

→

→ *Wheel 4 - Rear Left Wheel*

$$(3.2),(3.4) \xRightarrow{for\ i=4} \mathbf{V}_4 = \mathbf{V}_c + \boldsymbol{\omega} \times \mathbf{d}_4 \tag{3.15}$$

$$\xRightarrow{(3.3)(3.8)} \begin{cases} \mathbf{V}_{4x} = \mathbf{V}_{cx} + \boldsymbol{\omega} \times \left(-\frac{W}{2}\mathbf{k}\right) \\ \mathbf{V}_{4z} = \mathbf{V}_{cz} + \boldsymbol{\omega} \times \left(-\frac{L}{2}\mathbf{i}\right) \end{cases} \tag{3.16}$$

For the wheel motion, the driving angular velocity is represented with $\dot{\boldsymbol{\varphi}}_{\mathrm{i}}$, as shown in figure 2.3 and the steering wheel angle with $\boldsymbol{\vartheta}_{\mathrm{i}}$, for i=1,2,3,4, as shown in Figure 3.4.

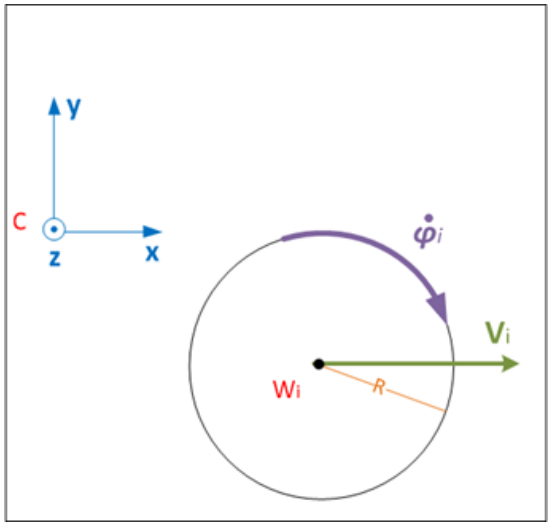

Figure 3.3 Driving angular velocity of the wheel (right side view)

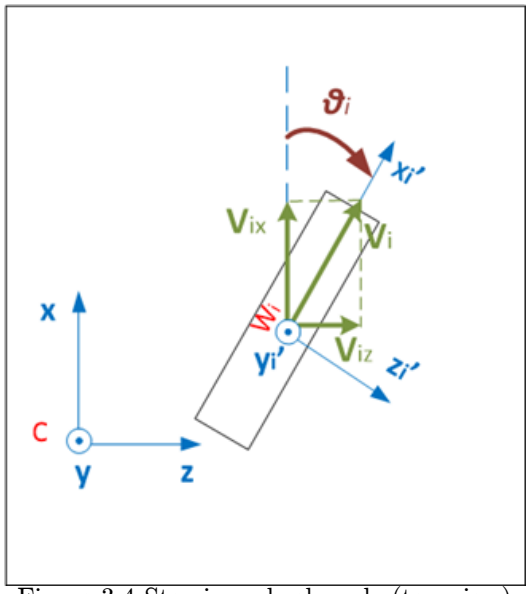

Figure 3.4 Steering wheel angle (top view)

The driving angular velocity $\dot{\boldsymbol{\varphi}}_i$, for $i = 1,2,3,4$, is positive clockwise for all the wheels with respect to the platform centre lateral axis and the steering angle $\boldsymbol{\vartheta}_i$, for $i = 1,2,3,4$, is positive clockwise with respect to the platform centre longitudinal axis.

In pure rolling conditions, the driving angular velocity $\dot{\boldsymbol{\varphi}}_i$ and the steering angle $\boldsymbol{\vartheta}_i$ for each wheel are calculated by the following equations:

$$|\dot{\boldsymbol{\varphi}}_{\boldsymbol{i}}| = \frac{\sqrt{\boldsymbol{V_{ix}}^{\boldsymbol{2}} + \boldsymbol{V_{iz}}^{\boldsymbol{2}}}}{\boldsymbol{R}} \tag{3.17}$$

$$\boldsymbol{\vartheta_i} = \boldsymbol{atan2}\left(\frac{\boldsymbol{V_{iz}}}{\boldsymbol{V_{ix}}}\right) \tag{3.18}$$

$$for\ i = 1,2,3,4, R: wheel\ radius$$

For the development of the algorithm based on inverse kinematic equations (3.17),(3.18) via (3.10)-(3.16), it is used as inputs the linear velocity and the angular velocity from the Joystick and the algorithm gives as outputs the driving angular velocity and the steering angle for each wheel, as shown in Figure 3.5.

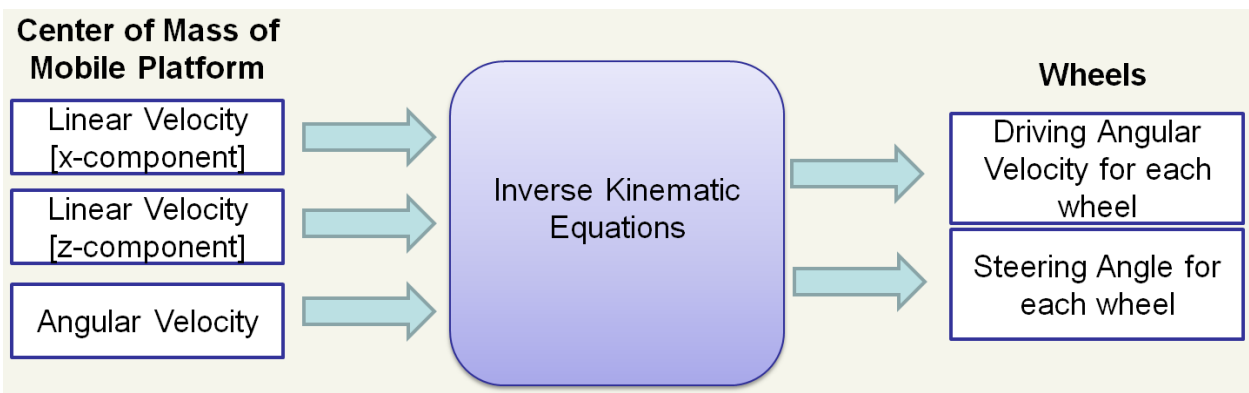

Figure 3.5 Diagram of inputs and outputs of the algorithm based on inverse kinematic equations

4 Permanent Magnet DC Motor

4.1 Mathematical model of PMDC motor

The permanent magnet DC motor is a system with electrical and mechanical components and a simplified equivalent representation is shown in Figure 4.1. The input of the system is the voltage that is applied to the motor's armature (V_{in}) and the output is the motor shaft angular speed (ω_m).

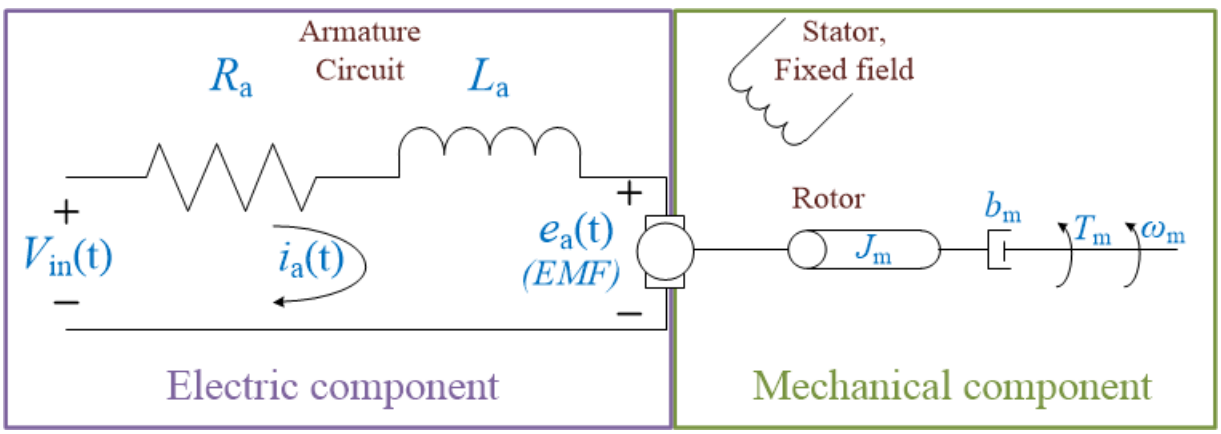

Figure 4.1 Schematic of an equivalent representation of the electromechanical components of the Permanent Magnet DC motor system

For the modeling of electrical characteristics of PMDC motor, applying Kirchkoff's voltage law to the armature circuit, the following equation yields:

$$\Sigma V = 0 \Rightarrow V_{in}(t) - R_a \cdot i_a(t) - L_a \cdot \frac{di_a}{dt} - e_a(t) = 0 \Rightarrow$$

$$R_a \cdot i_a(t) + L_a \cdot \frac{di_a}{dt} = V_{in}(t) - e_a(t) \tag{4.1}$$

where R_a: armature resistance (Ohm), L_a: armature inductance (Henry), $i_a(t)$: armature current (Ampere), $e_a(t)$: back electromotive force - EMF voltage (Volt).

The back EMF voltage $e_{\mathrm{a}}(t)$ is proportional to the motor shaft angular speed (ω_m), given by the equation:

$$e_{\mathrm{a}}(t) = K_e \cdot \omega_m(t) \tag{4.2}$$

where K_e: back EMF constant ($\mathrm{V \cdot s/rad}$).

For the modeling of mechanical characteristics of PMDC motor, applying Newton's 2nd law of motion for rotational systems to the mechanical components, the following equation yields:

$$\Sigma T = J_{\mathrm{m}} \cdot \frac{\mathrm{d}\omega_{\mathrm{m}}}{\mathrm{dt}} \Rightarrow T_e - T_f - T_L = J_{\mathrm{m}} \cdot \frac{\mathrm{d}\omega_{\mathrm{m}}}{\mathrm{dt}} \tag{4.3}$$

where J_{m}: moment of inertia of rotor ($\mathrm{kg \cdot m^2}$), T_e: electromagnetic torque (N·m), T_f: frictional torque (N·m), T_L: torque of the mechanical load (N·m).

The electromagnetic torque is proportional to the armature current for the PMDC motor and given by the equation:

$$T_e = K_{\mathrm{t}} \cdot i_{\mathrm{a}}(t) \tag{4.4}$$

where K_{t}: torque factor constant ($\mathrm{N \cdot m/A}$).

The frictional torque is proportional to the angular velocity of the motor shaft and given by the following equation:

$$T_f = b_{\mathrm{m}} \cdot \omega_m(t) \tag{4.5}$$

where b_{m}: motor viscous friction constant (N·m· s).

Between the motor and the load, gears are connected. Gear ratio (K_g) is the number of teeth on the driven gear (at the load side) divided by the number of teeth on the drive gear (at the motor side). The torque of the mechanical load is equal to:

$$T_L = \frac{J_L}{{K_g}^2} \cdot \frac{\mathrm{d}\omega_\mathrm{m}}{\mathrm{dt}} + \frac{b_L}{{K_g}^2} \cdot \omega_m(t) \tag{4.6}$$

where J_L: moment of inertia of the mechanical load ($\mathrm{kg} \cdot \mathrm{m}^2$) and b_L: viscous friction constant of the mechanical load (N·m· s).

The equation(4.3) due to the equations(4.4)-(4.6)gives:

$$K_\mathrm{t} \cdot i_\mathrm{a}(t) - b_\mathrm{m} \cdot \omega_m(t) - \frac{J_L}{{K_g}^2} \cdot \frac{\mathrm{d}\omega_\mathrm{m}}{\mathrm{dt}} - \frac{b_L}{{K_g}^2} \cdot \omega_m(t) = J_\mathrm{m} \cdot \frac{\mathrm{d}\omega_\mathrm{m}}{\mathrm{dt}} \Rightarrow$$

$$K_\mathrm{t} \cdot i_\mathrm{a}(t) = b_\mathrm{eq} \cdot \omega_m(t) + J_\mathrm{eq} \cdot \frac{\mathrm{d}\omega_\mathrm{m}}{\mathrm{dt}} \tag{4.7}$$

where $J_\mathrm{eq} = J_\mathrm{m} + \frac{J_L}{{K_g}^2}$ and $b_\mathrm{eq} = b_\mathrm{m} + \frac{b_L}{{K_g}^2}$.

Taking the Laplace transform, the equations are:

$$(4.1)\ \&\ (4.2) \xRightarrow{Laplace} V_{in}(s) = R_\mathrm{a} \cdot I_\mathrm{a}(s) + L_\mathrm{a} \cdot s \cdot I_\mathrm{a}(s) + K_e \cdot \omega_m(s) \tag{4.8}$$

$$(4.7) \xRightarrow{Laplace} K_\mathrm{t} \cdot I_\mathrm{a}(s) = b_\mathrm{eq} \cdot \omega_m(s) + J_\mathrm{eq} \cdot s \cdot \omega_m(s) \tag{4.9}$$

The transfer function of the output motor shaft angular velocity (rad/sec) to input voltage is denoted by:

$$(4.8),(4.9) \Rightarrow G_m(s) = \frac{\omega_m(s)}{V_{in}(s)} = \frac{K_t}{L_a \cdot J_{eq} \cdot s^2 + (R_a \cdot J_{eq} + L_a \cdot b_{eq})s + (R_a \cdot b_{eq} + K_t \cdot K_e)} \tag{4.10}$$

The transfer function of the output angular velocity (rad/sec) of the mechanical load to input voltage of the motor is given by the following equation:

$$\xrightarrow{K_g = \frac{\omega_m(s)}{\omega_L(s)}} G_L(s) = \frac{\omega_L(s)}{V_{in}(s)} = \frac{K_t/K_g}{L_a \cdot J_{eq} \cdot s^2 + (R_a \cdot J_{eq} + L_a \cdot b_{eq})s + (R_a \cdot b_{eq} + K_t \cdot K_e)} \tag{4.11}$$

4.2 Mathematical model of the driving PMDC motor

For the driving system of the mobile platform, the hub wheel motor 400-T Swissdrive has been selected. The following nominal values for the various parameters of the PMDC motor used:

- → *armature resistance* $R_a = 0.15\ Ohm$
- → *armature inductance* $L_a = 0.12\ H$
- → *torque factor constant* $K_t = 1.22\ N \cdot m/A$
- → *back EMF constant* $K_e = 1.22\ \ V \cdot s/rad$
- → *equivalent inertia* $J_{eq} = 0.001\ kg \cdot m^2$
- → *equivalent viscous friction constant* $b_{eq} = 1.5\ N{\cdot}m{\cdot}\ s$
- → *gear ratio* $K_g = 8.786$

Substituting the above values on the equation (4.11), the transfer function of the output angular velocity of the mechanical load to input voltage of the motor is given by the following equation:

$$G_L(s) = \frac{\omega_L(s)}{V_{in}(s)} = \frac{0.1389}{0.00012 \cdot s^2 + 0.18015s + 1.7134} \tag{4.12}$$

5 Control of Mobile Platform

5.1 Fuzzy logic position control of steering DC Motor

Fuzzy logic controller is a rule based system. Fuzzy logic controllers can be designed and implemented for a motor without any prior the knowledge of the motor and its load characteristics [24]. In this thesis, due to lack of information of the motor and its load characteristics, the steering angle position control of the wheel is implemented with fuzzy logic controller. A schematic of the fuzzy logic controller is shown in Figure 5.1. The fuzzy controller has three stages: fuzzyfication, inference engine and defuzzyfication.

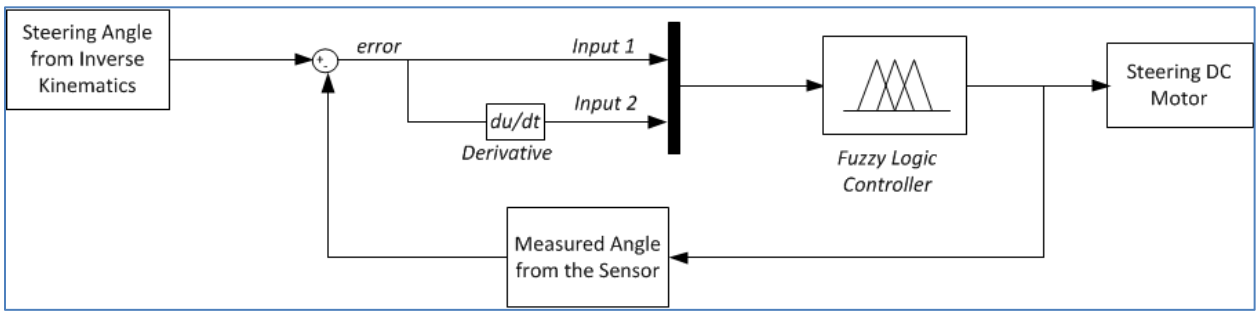

Figure 5.1 Schematic of the fuzzy logic controller of steering DC motor

The designed fuzzy logic controller has two inputs (fuzzyfication) and one output (defuzzyfication). The first input is the position error $e(t) = \vartheta_{ref}(t) - \vartheta(t)$, where $\vartheta_{ref}(t)$ is the desire steering angle of the wheel calculated from the inverse kinematics and $\vartheta(t)$ is the actual steering angle measured from the angle sensor. The variables of the input are shown in Figure 5.2. The second input is the error change or derivative of the error $de(t)$, as shown in Figure 5.3. The output of the fuzzy logic controller is the control voltage (Figure 5.4). The linguistic variables are defined as NB: Negative Big, NM: Negative Medium, NS: Negative Small, ZE: Zero, PS: Positive Small, PM: Positive Medium, PB: Positive Big.

Figure 5.5 illustrates the method used in reaching the desired value. For example, at stage A (Figure 5.5), the error is positive and the error change is negative, which means that the response is heading in the correct direction and the fuzzy logic controller will continue in this direction, but at stage B (Figure 5.5), the error is negative and the error change is big negative, so the response is heading in the wrong direction and the fuzzy logic controller will change its direction [25].

The set of decision rules (inference engine) is shown in Table 5-1. The fuzzy rules contain the relationships between inputs and output. Each control input has 7 fuzzy sets so there are 49 fuzzy rules. The fuzzyfication and inference system were designed experimentally. The rule base structure is Mamdani fuzzy interference reasoning.

The fuzzy control rule is in the form of: If $e = Ei$ and $de = dEi$ then voltage$= V(i,j)$. For example if error is PM and error change is PM then the output (voltage) is PB. In that case, the motor will rotate with high angular speed until the position error is smaller.

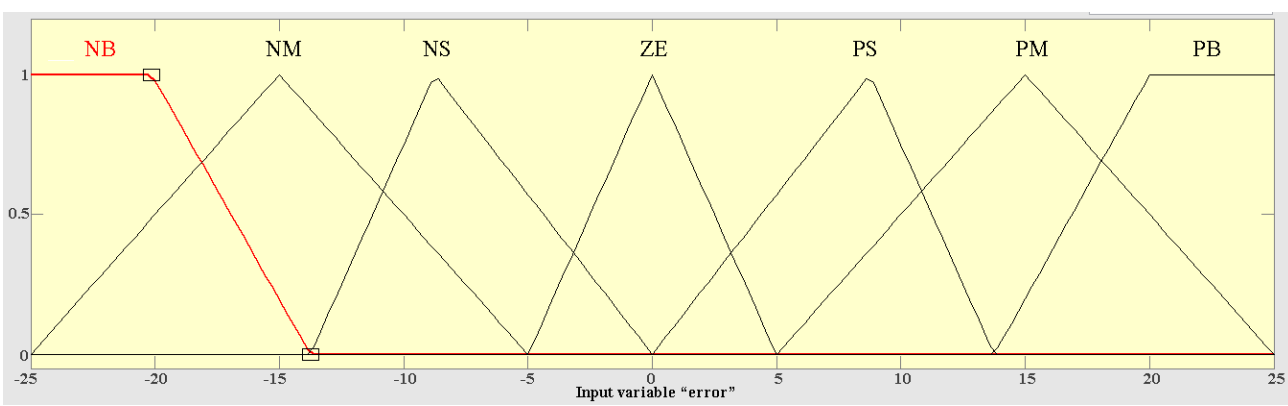

Figure 5.2 Membership function of input "error"

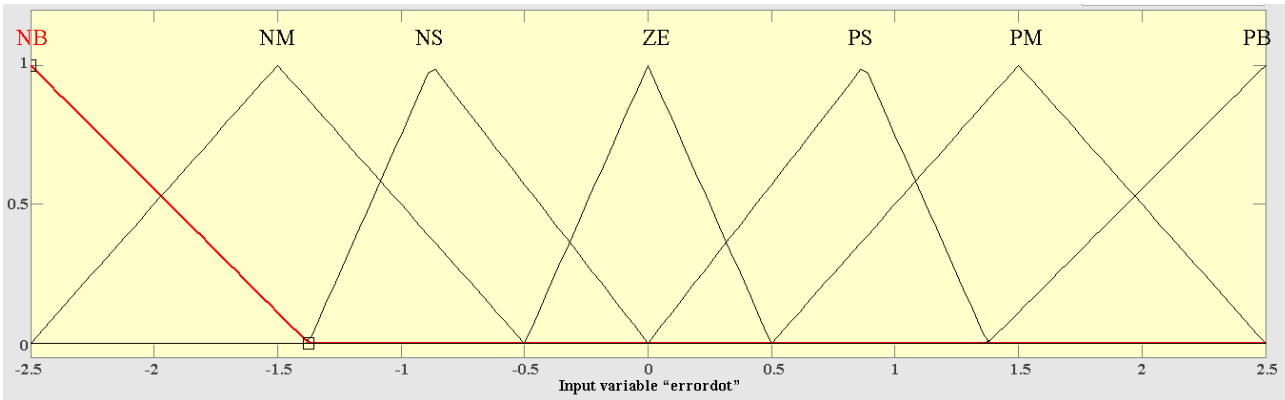

Figure 5.3 Membership function of input "error change"

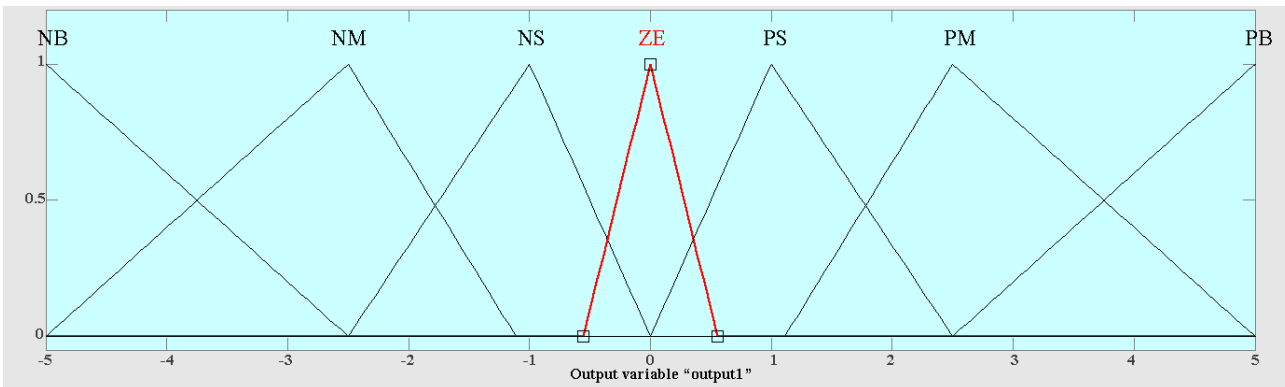

Figure 5.4 Membership function of output "Voltage"

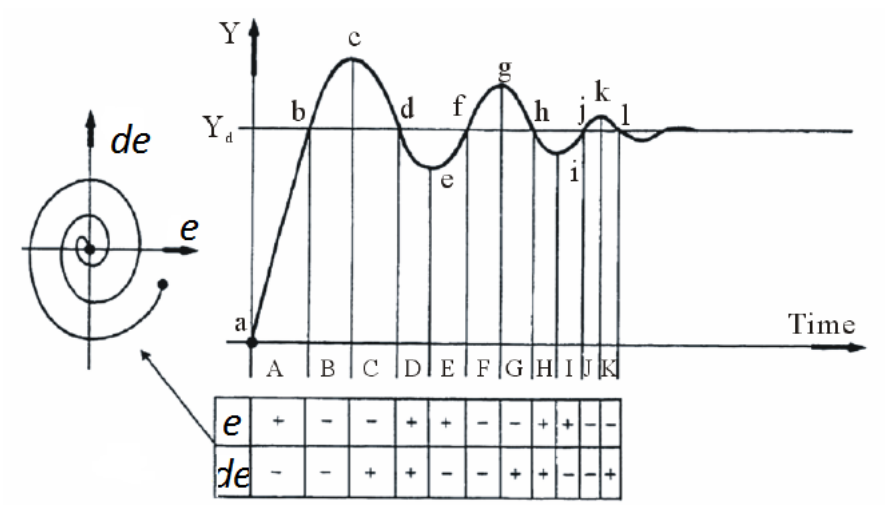

Figure 5.5 Error and error change approach in fuzzy logic control [25]

Table 5-1: Fuzzy rule base

de\e	NB	NM	NS	ZE	PS	PM	PB
NB	NB	NB	NB	NB	NM	NS	ZE
NM	NB	NB	NM	NM	NS	ZE	PS
NS	NB	NM	NS	NS	ZE	PS	PM
ZE	NB	NM	NS	ZE	PS	PM	PB
PS	NM	NS	ZE	PS	PS	PM	PB
PM	NS	ZE	PS	PM	PM	PB	PB
PB	ZE	PS	PM	PB	PB	PB	PB

5.2 PI speed control of driving DC motor - Simulation results

A PI controller was used for the speed control of hub wheel motor 400-T Swissdrive. The transfer function of the motor was computed using the mathematical model, described in chapter 4.2. In order to choose the proportional and the integral gains, the PID controller tuning of mathworks matlab/Simulink control system toolbox was used. In Figure 5.6 the Simulink model of the PID DC motor speed control system is shown.

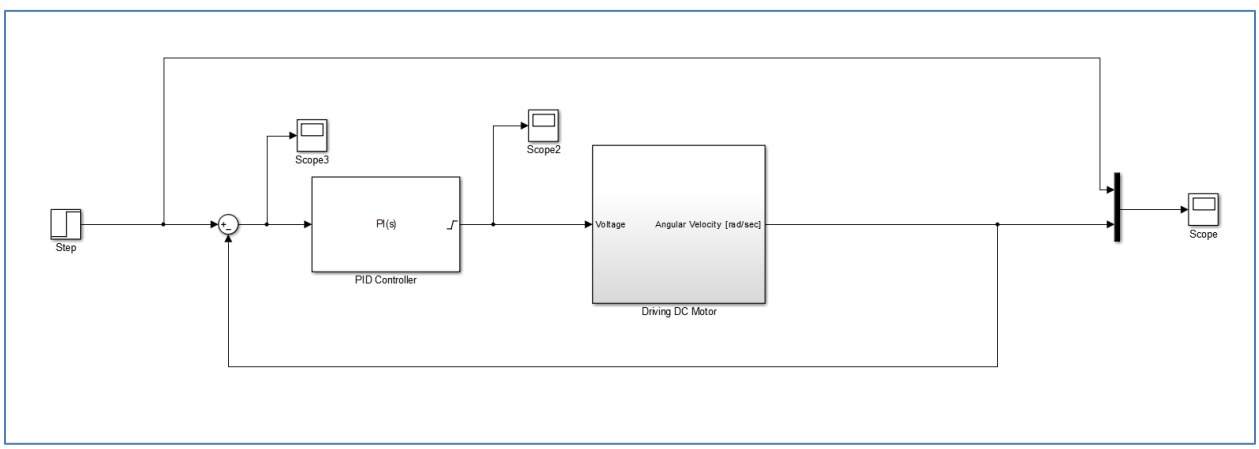

Figure 5.6 Simulink model of PID DC motor speed control system

After using the PID controller tuning and adjusting the values of the proportional and integral gain, the following values were achieving the desired performance:

→ Proportional gain $K_P = 0.9$

→ Integral gain $K_I = 25$

In Figure 5.7, the simulation results are shown. The reference signal (desired speed) is in blue and the system's output speed is in green.

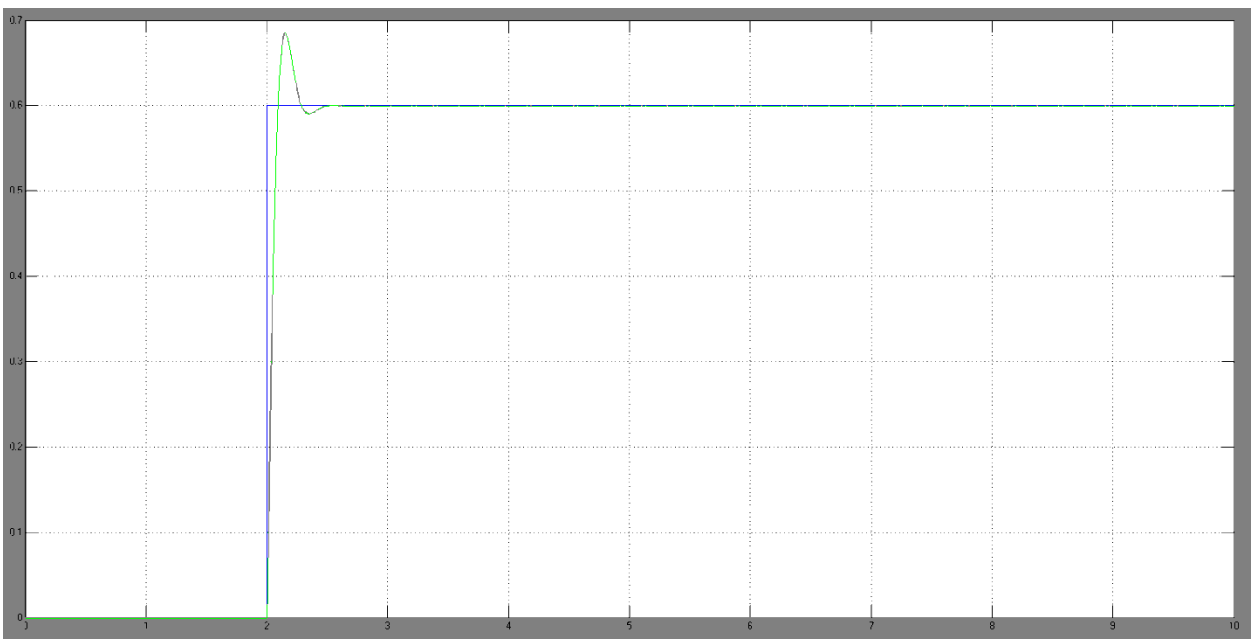

Figure 5.7 Reference speed (blue) and system speed output (green)

5.3 Implementation of the control of the mobile platform

In this section, the algorithm of the control of the mobile platform is explained. In Figure 5.8, the diagram of the control of the mobile platform is presented. Using joystick as input, the inverse kinematics algorithm receives the signals for the linear and angular velocity for the center of the mass of the mobile platform. The joystick JC2000 only gives the x-component and the z-component of the linear velocity and does not support rotation. The axes of the mobile platform have been defined in chapter 3. In order to test the inverse kinematics algorithm for rotation, one channel of the joystick is used to represent angular velocity.

The joystick signals are the inputs of the inverse kinematics algorithm. The outputs of the inverse kinematics algorithm are the steering angle and driving angular velocity for each wheel. The steering angle is limited in the space (-90°, 90°], because the hub wheel motor 400-T is able to drive in 2 directions - forward and backwards (reverse). Additionally, the steering angle is kept the same until a new command from the joystick comes. Due to those limitations, an adapted algorithm has been implemented which generates the adapted steering angle and adapted driving angular velocity for each wheel.

The adapted values are used as references (set points) for the control loops that have already described in chapters 5.1**Error! Reference source not found.** and 5.2.

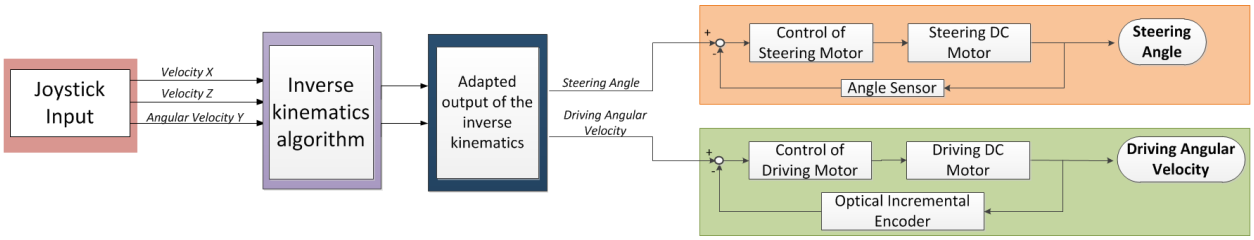

Figure 5.8 Diagram of the control of the mobile platform

6 Experimental Results

6.1 Steering of mobile platform wheels

In this section, experimental results obtained in real-world steering of CORBYS mobile platform wheels using designed controller are presented.

6.1.1 Scenario A - Linear Motion of the mobile platform

In the considered experimental scenario, so-called "Linear Motion of mobile platform", the mobile platform steers in directions forward, backward and sideways, using joystick as input device. The system receives two signals from the joystick, as shown in Figure 6.1. The first signal represents the linear velocity in x-axis, which means forward and backward (Figure 6.1.A) and the second signal represents the linear velocity in z-axis (Figure 6.1.B). The axes of the mobile platform have been defined in chapter 3.

From the joystick signals (Figure 6.1), the wheels of the mobile platform should steer as following: the wheels should steer in forward direction from 6 till 14.5 sec (Motion I), the wheels should steer towards the right direction from 15.5 till 23 sec (Motion II), the wheels should steer in backward direction from 24 till 37.5 sec (Motion III), the wheels should steer towards the left direction from 38 till 48 sec (Motion IV) and the wheels should not move for the rest time.

Starting from the input joystick signals, the output of the inverse kinematics was calculated as shown in Figure 6.2A for one of the mobile platform wheels. Since the desired motion of the platform is linear, all the wheels should have the same steering angle. For that reason, the steering angle of one wheel is presented in Figure 6.2A. As it can be seen, the output of the inverse kinematics are angles 0°, 90°, 180° and -90° for the Motions I, II, III and IV, respectively.

Figure 6.2B shows the adapted output of the inverse kinematics. Namely, since the driving DC motors are able to drive in 2 directions - forward and backwards (reverse), the value of steering angle is limited in the space (-90°, 90°]. For example, in motion III the platform should move backwards. In that case there are two options: to steer the wheel at 180 degrees and drive forward or to steer the wheel at 0 degrees and drive backwards. With the limitation of steering angle, the second option will be chosen. Additionally, the steering angle is not changing until it gets a new command from the joystick. So between motion II and III and motion III and IV the steering angle does not go to 0 degrees but keeps the previous value (Figure 6.2.B).

The calculated steering angle is the reference signal for the control of the steering DC motor. The reference signal and the actual steering angle, measured from the angle sensors, for each wheel are given Figure 6.3. From the results, it is clear that the fuzzy logic controller eliminates the error and the steering DC motor steers with maximum speed when the error is big, so it is time efficient.

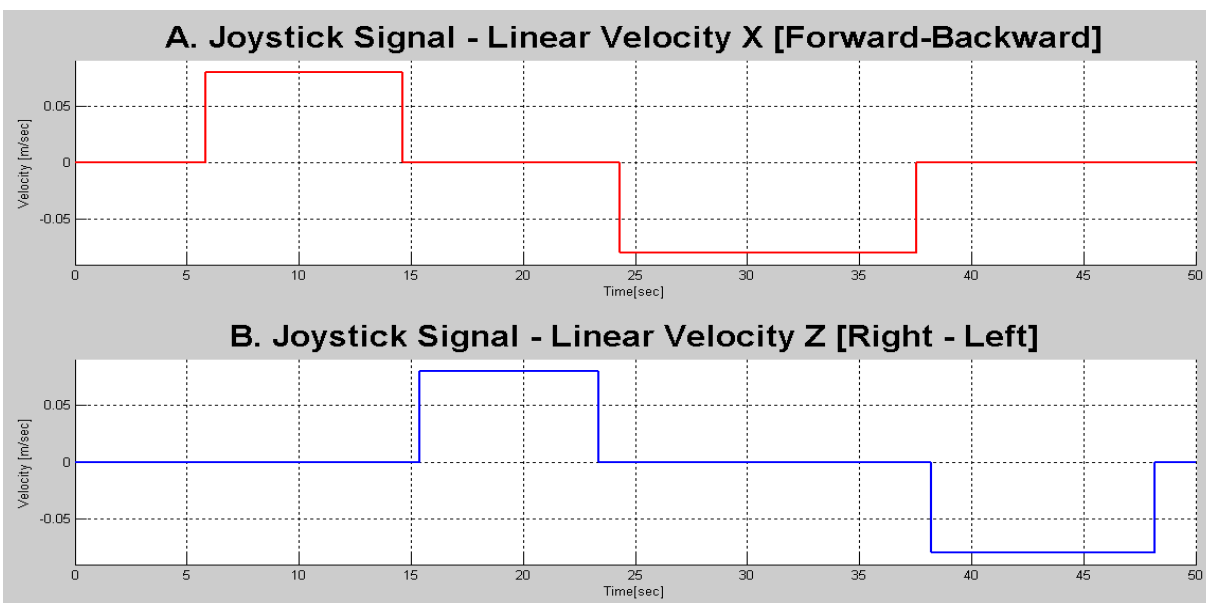

Figure 6.1 Joystick Signals

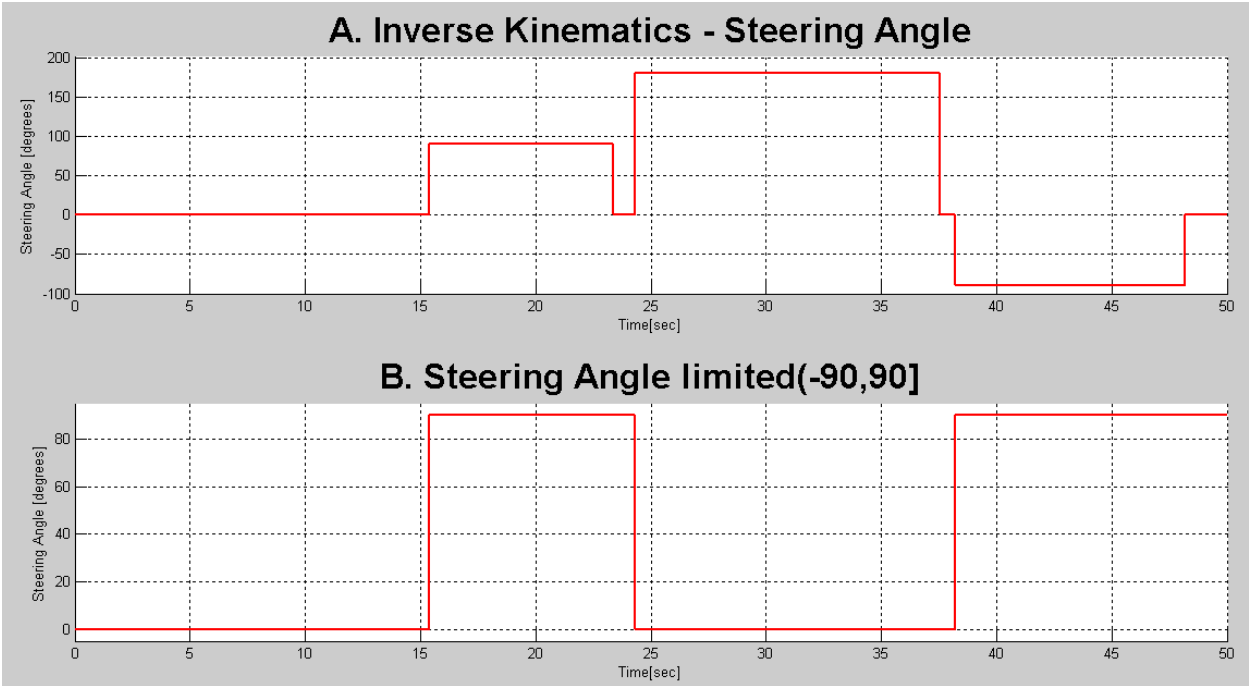

Figure 6.2 Calculated Steering Angle

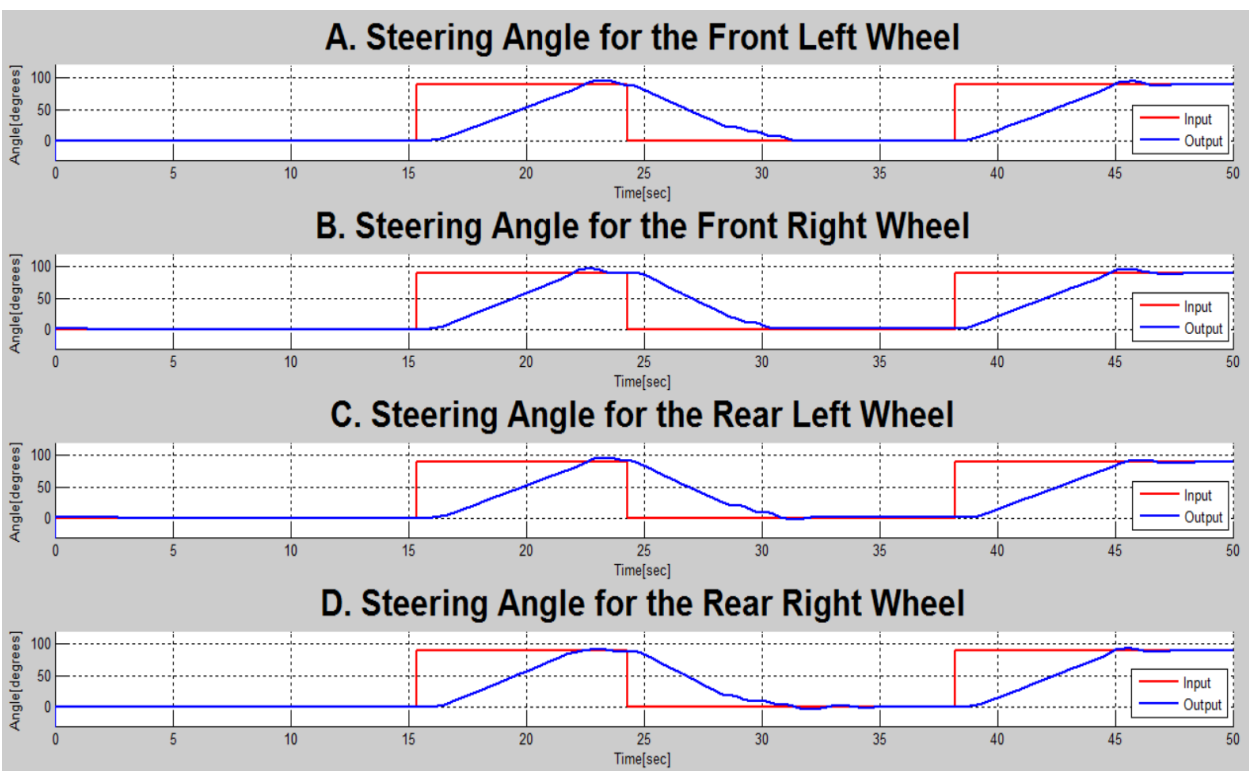

Figure 6.3 Reference (red) and Measured (blue) steering angles

6.1.2 Scenario B - Rotation of the mobile platform

In the following experimental scenario, so-called "Rotation of mobile platform", the mobile platform exhibits a rotation around its y-axis, using joystick as input device. The system receives one signal from the joystick, as shown in figure 5.4 and represents the angular velocity around the center of the mass of the mobile platform.

From the joystick signals (Figure 6.4), the mobile platform should move as following: the platform should rotate clockwise around the center of mass from 5 until 7.1 sec (Motion I), the platform should rotate counterclockwise around the center of mass from 8.2 until 8.6 sec and from 9.9 until 11 sec (Motion II and III) and the platform should not move for the rest time.

Using the signal from the joystick as input, the output of the inverse kinematics was calculated as shown in Figure 6.5 for each wheel of the mobile platform. Namely, since the driving DC motors are able to drive in 2 directions - forward and backwards, the value of steering angle is limited to (-90°, 90°]. Additionally, the steering angle is not changing until it gets a new command from the joystick. The adapted output of the inverse kinematics can be seen in Figure 6.6 (red signal). In this scenario, the front right wheel and rear left wheel steer at 59 degrees and the front left wheel and rear right wheel steer at -59 degrees.

The calculated steering angle is the reference signal for the control of the steering DC motor. The reference signal and the actual steering angle, measured from the angle sensors, for each wheel are given in Figure 6.6. In this scenario, also, the results of fuzzy logic controller are efficient.

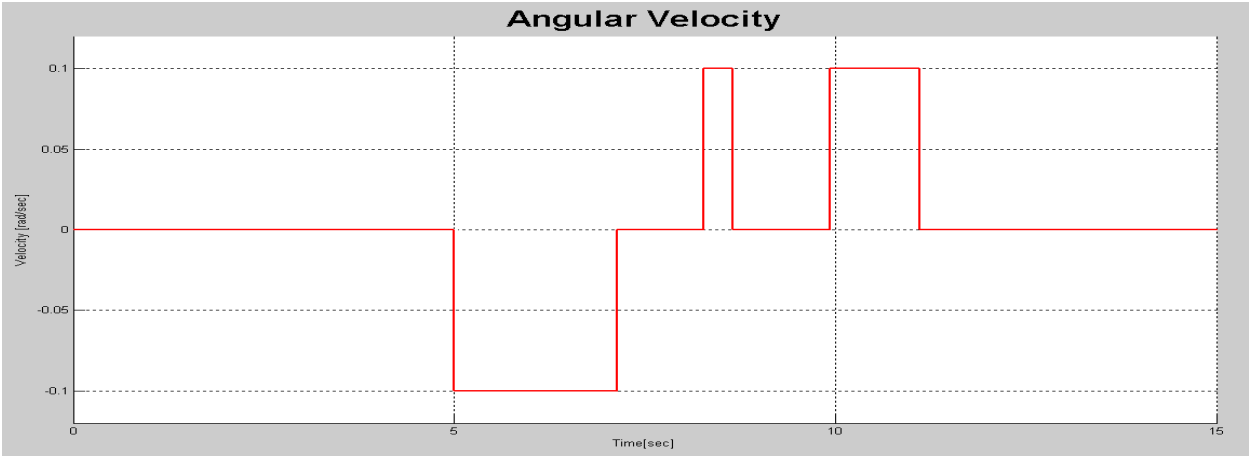

Figure 6.4 Joystick Signal

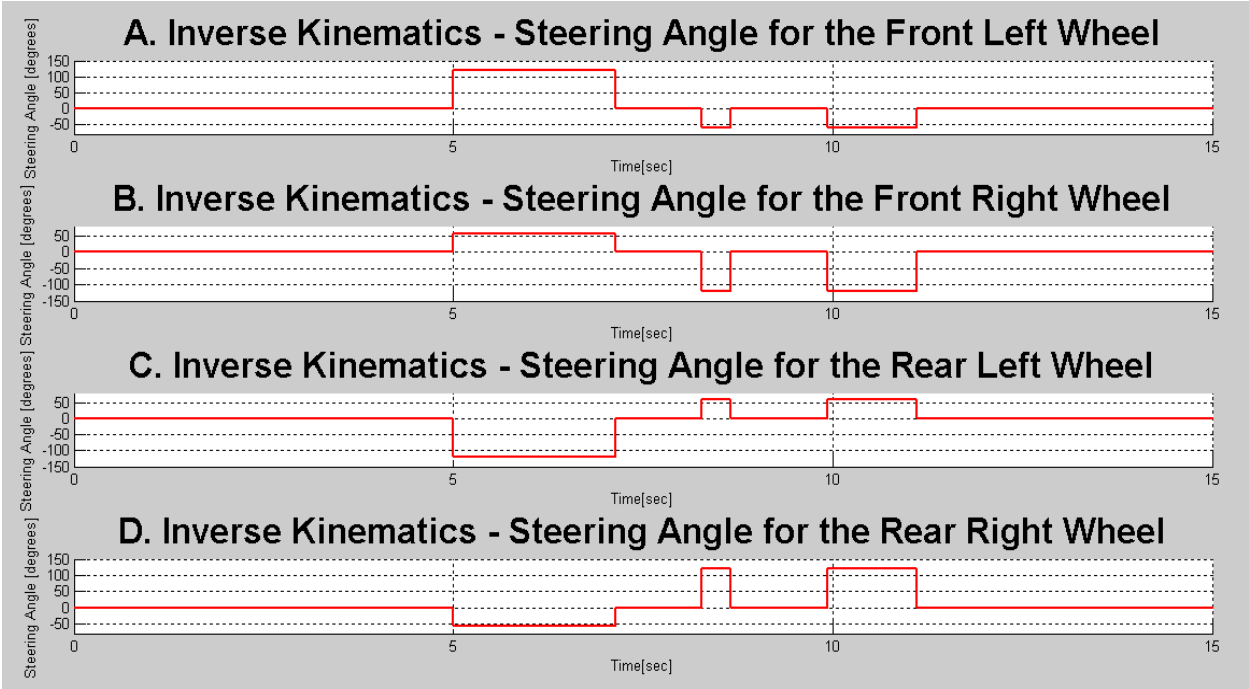

Figure 6.5 Calculated Steering Angle

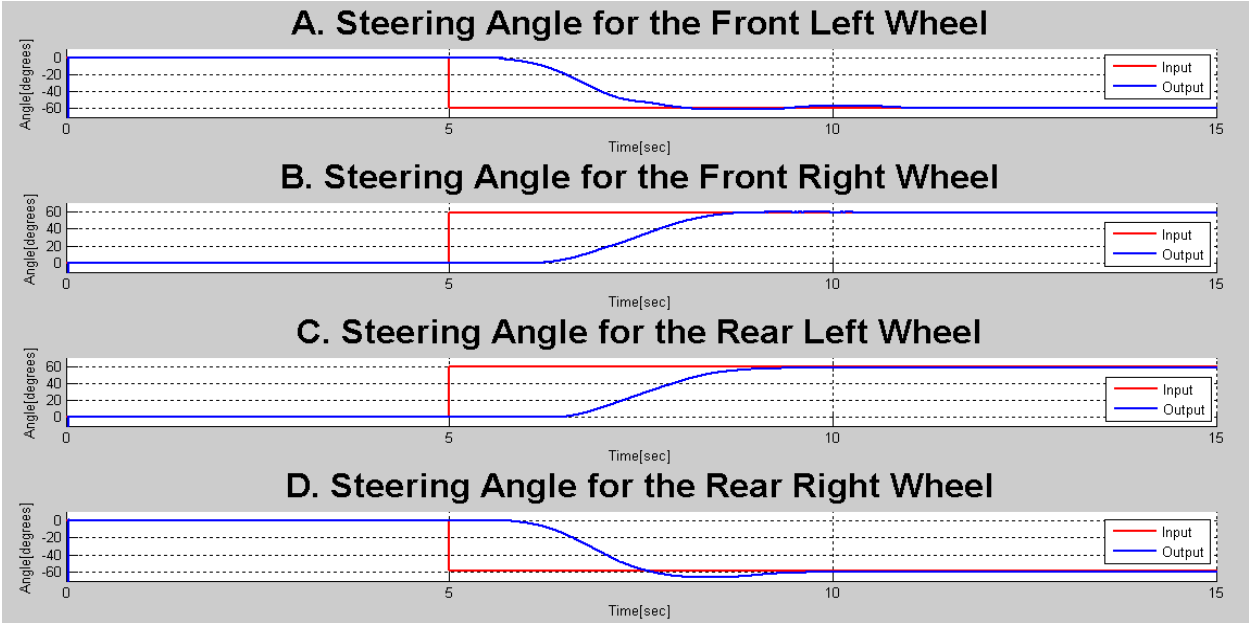

Figure 6.6 Reference (red) and Measured (blue) steering angles

6.2 Driving of the mobile platform

In the considered experimental scenario, so-called "driving of the mobile platform", experimental results obtained in real-world steering and driving of CORBYS mobile platform using designed controllers are presented. The mobile platform moves in directions forward, backward and sideways, using joystick as input device. The system receives two signals from the joystick, as shown in Figure 6.7. The first signal represents the linear velocity in x-axis, which means forward and backward (Figure 6.7A) and the second signal represents the linear velocity in z-axis (Figure 6.7.B). The axes of the mobile platform have been defined in chapter 3.

From the joystick signals (Figure 6.7), the mobile platform should move as following: the mobile platform should move in forward direction from 11.5 till 15 sec (Motion I), then it should move backwards from 17.5 till 19 sec (Motion II). Afterwards it should move towards the left direction from 22.5 till 28 sec (Motion III) and in forward direction from 35 till 43.5 sec (Motion IV) and the mobile platform should not move for the rest time.

Starting from the input joystick signals, the outputs of the inverse kinematics were calculated as shown in Figure 6.8A and Figure 6.10A for one of the mobile platform wheels. Since the desired motion of the platform is linear in the scenario, all the wheels should have the same steering angle and same driving angular velocity. For that reason, the steering angle of one wheel is presented in Figure 6.8Aand the angular velocity of one wheel is presented in Figure 6.10A. As it can be seen in Figure 6.8A, the output of the inverse kinematics are angles 0°, 180°, -90° and 0° for the Motions I, II, III and IV, respectively.

Figure 6.8B shows the adapted output of the steering angle of the inverse kinematics. Namely, since the driving DC motors are able to drive in 2 directions - forward and backwards (reverse), the value of steering angle is limited in the space (-90°, 90°]. Additionally, the steering angle is not changing until it gets a new command from the joystick. Figure 6.10B shows the adapted output of the driving angular velocity. So, for

example, in motion III the platform should move towards the left side. In that case there are two options: to steer the wheel at -90° degrees and drive forward or to steer the wheel at 90 degrees and drive backwards. With the limitation of steering angle, the second option will be chosen, as it is shown in Figure 6.10B.

The calculated steering angle is the reference signal for the control of the steering DC motor. The reference signal and the actual steering angle, measured from the angle sensors, for each wheel are given in Figure 6.9.

The calculated driving angular velocity is the reference signal for the control of the steering DC motor. The reference signal and the actual angular velocity, measured from the encoder, for each wheel are given in Figure 6.11.

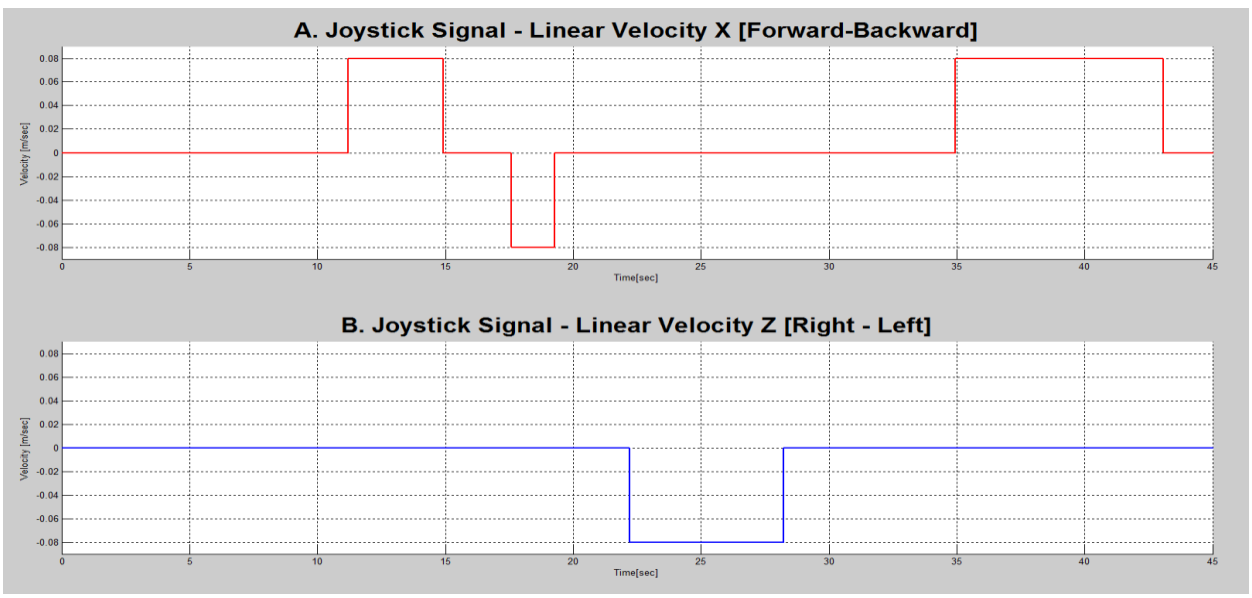

Figure 6.7 Joystick Signals

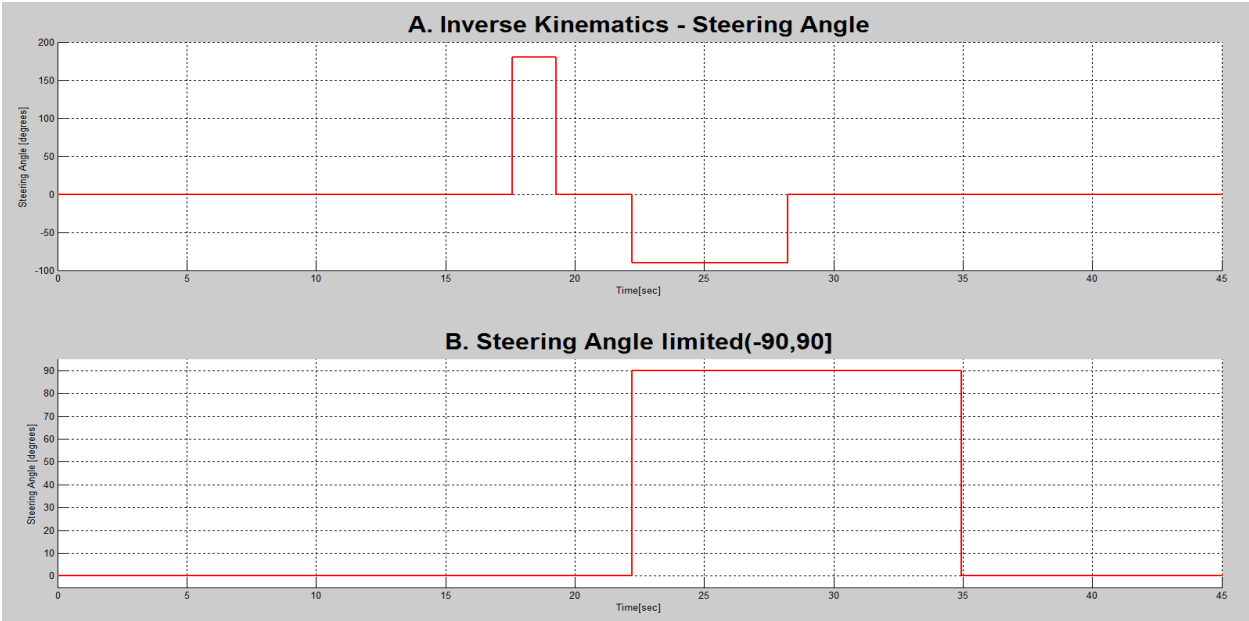

Figure 6.8 Calculated Steering Angle

Figure 6.9 Reference (red) and Measured (blue) steering angles

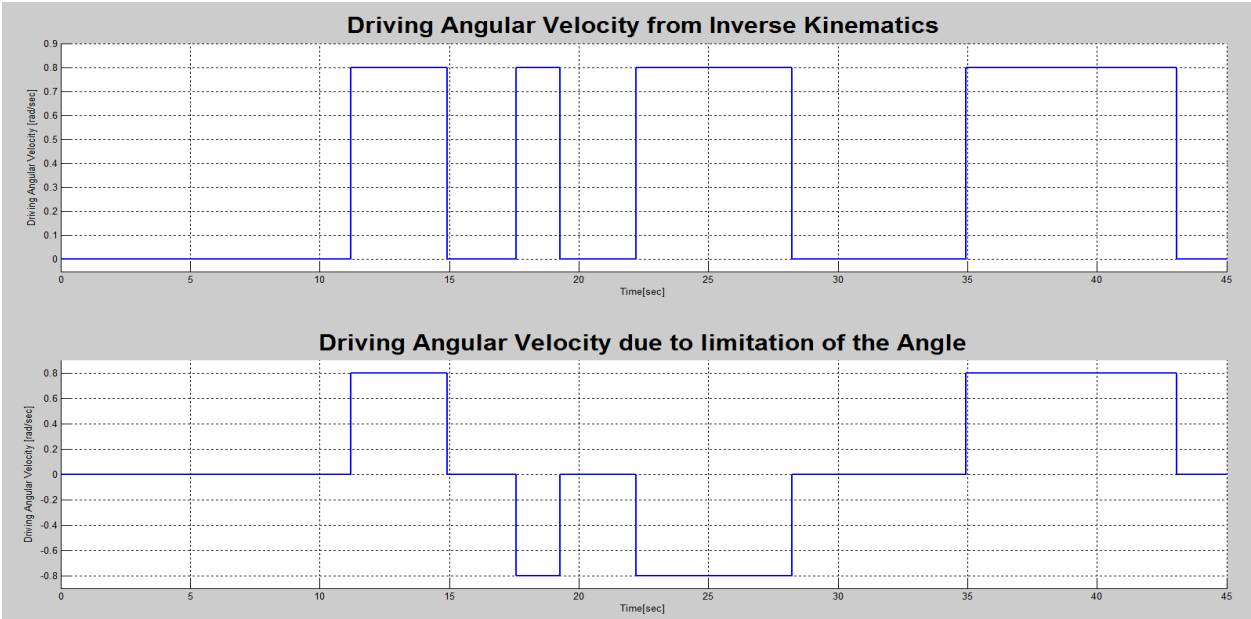

Figure 6.10 Calculated driving angular velocity

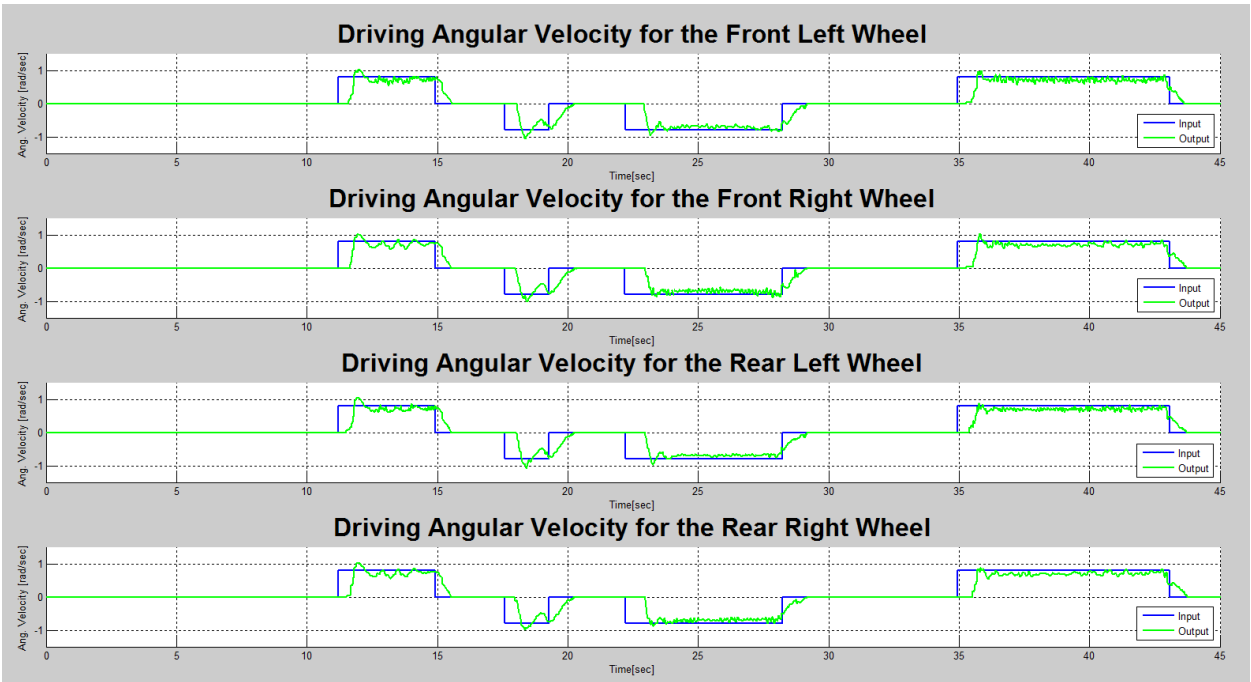

Figure 6.11 Reference (blue) and Measured (green) driving angular velocity

7 Conclusion and Future Work

7.1 Conclusion

In this thesis, an inverse kinematics based algorithm was developed and the mobile platform was maneuvered successfully using a joystick. The real-world experimental results of mobile platform steering using the fuzzy logic controller exhibited a very high degree of accuracy (less than 2 degrees error). Additionally a high speed of the control was achieved as steering DC motor was able to rotate with maximum speed until it got really close to the desire position, so the control was time efficient.

7.2 Future work

For further work, the inverse kinematics based algorithm could be altered in order to receive the velocity input from the pelvis link (from the patient). In that case, the input will not be the velocity in the center of the mass but the velocity of the patient. Additionally, in order to eliminate overshoots and undershoots that has been observed in fuzzy logic position control of DC motor, a Fuzzy PID control could be implemented.

8 Bibliography

[1] S. Slavnić, C. Glackin C. D. Ristić-Durrant, "CORBYS project overview: approach and achieved results," *W. Jensen et al. (eds), Replace, Repair, Restore, Relieve – Bridging Clinical and Engineering Solutions*, pp. 139-147, 2014.

[2] (2014, July) CORBYS. [Online]. www.corbys.eu

[3] D. Ristić-Durrant, R. Tschakarow, T. Brendel, M. Tüttemann., A. Leu, A. Gräser S. Slavnić S., "Mobile robotic gait rehabilitation system CORBYS – overview and first results on orthosis actuation," in *IEEE/RSJ International Conference on Intelligent Robots and Systems (IROS)*, Chicago, 2014.

[4] EtherCAT Technology Group. (2014) EtherCAT. [Online]. http://www.ethercat.de/en/technology.html

[5] (2014, January) Position and Measurement Control Hardware - Penny + Giles. [Online]. http://www.pennyandgiles.com/getattachment/a6bb9db0-f4be-47c9-8e9d-e8931694969f/JC2000˙jun07(EN)

[6] Inc. Curtis Instruments, Electronic Motor Controllers Models 1212 & 1212P Manual, 2013.

[7] Micro-Motor AG, Hub wheel motor 400-T , 2010.

[8] Aginlent Technologies, Technical Data: HEDS-9000/9100/9200 Extended Resolution Series, 2002.

[9] novotechnik, Datasheet: Series RFC4800, NOVOHALL Rotary Sensor, 2013.

[10] BECKHOFF, Documentation for EtherCAT Bus Coupler EK110-EK15xx, 2014.

[11] BECKHOFF, Documentation for Incremental Encoder Interface EL5101, 2013.

[12] BECKHOFF, Documentation for Digital Output Terminals EL20xx˙EL2124, 2013.

[13] BECKHOFF, Documentation for 2 Channel Analog Output Terminals, 16 bit. EL41xxen, 2014.

[14] BECKHOFF, Documentation for Analog Input Terminals (16 bit), 2014.

[15] Inc. The MathWorks. (2014) Simulink Real-Time Overview. [Online]. http://www.mathworks.com/products/simulink-real-time/index.html

[16] S. Omatu, M. Yoshioka, and T. Kosaka, "PID Control of Speed and Torque of Electric Vehicle," in *Third International Conference on Advanced Engineering Computing and Applications in Sciences*, Sliema, 2009, pp. 157-162.

[17] Huihuan Qian, Yangsheng Xu, and Guoqing Xu Tin Lun Lam, "Omni-directional steer-by-wire interface for four wheel independent steering vehicle," in *IEEE International Conference on Robotics and Automation*, Kobe, 2009, pp. 1383- 1388.

[18] Tian Li, Gao Hong Xiao Ping, "Research on Four-wheel-Steering Automobile based on Simulated Annealing PID algorithm," in *Third International Conference on Intelligent System Design and Engineering Applications (ISDEA)*, Hong Kong, 2013, pp. 1175-1178.

[19] N. Hamzah, Y.M. Sam, H. Selamat, M.K. Aripin, and M.F. Ismail, "Yaw Stability Improvement for Four-Wheel Active Steering Vehicle using Sliding Mode Control ," in *IEEE 8th International Colloquium on Signal Processing and its Applications (CSPA)*, Melaka, 2012, pp. 127 - 132.

[20] Zhang Junyou Wang Shufeng, "The Research and Application of Fuzzy Control in Four-wheel-steering Vehicle," in *Seventh International Conference on Fuzzy Systems and Knowledge Discovery (FSKD)*, Yantai, 2010, pp. 1397-1401.

[21] L. Zadeh, "Fuzzy sets," *Information and Control*, vol. 8, pp. 338-353, 1965.

[22] Chennakesava R. Alavala, "Fuzzy Logic and Neural Networks," *New Age International Publishers*, 2008.

[23] Shuocheng Lee Guoshing Huang, "PC-based PID Speed Control in DC Motor," in *International Conference on Audio, Language and Image Processing,* Shanghai, 2008, pp. 400-407.

[24] C.Senthil Kumar N.Senthil Kumar, "Design and Implementation of Adaptive Fuzzy Controller for Speed Control of Brushless DC Motors," *International Journal of Computer Applications*, vol. 1, no. 27, pp. 36-41, 2010.

[25] B. Hamed and M. Al-Mobaied, "Fuzzy PID Controllers Using FPGA Technique for Real Time DC Motor Speed Control," *Intelligent Control and Automation*, vol. 2, no. 3, pp. 233-240, 2011.

[26] Cognitive Control Framework for Robotic System (CORBYS). [Online]. http://www.corbys.eu/

[27] W. Shufeng and Z. Junyou, "The Research and Application of Fuzzy Control in Four-wheel-steering Vehicle," in *Seventh International Conference on Fuzzy Systems and Knowledge Discovery (FSKD)*, Yantai, 2010, pp. 1397-1401.